

Human V2A: A map of the peripheral visual hemifield with functional connections to scene-selective cortex

Joris A. Elshout

Department of Cognitive Neuroscience,
Radboud University Medical Centre,
Nijmegen, the Netherlands
Donders Institute for Brain, Cognition and Behaviour,
Centre for Cognitive Neuroimaging, Radboud University,
Nijmegen, the Netherlands



Albert V. van den Berg

Department of Cognitive Neuroscience,
Radboud University Medical Centre,
Nijmegen, the Netherlands
Donders Institute for Brain, Cognition and Behaviour,
Centre for Cognitive Neuroimaging, Radboud University,
Nijmegen, the Netherlands

Koen V. Haak

Department of Cognitive Neuroscience,
Radboud University Medical Centre,
Nijmegen, the Netherlands
Donders Institute for Brain, Cognition and Behaviour,
Centre for Cognitive Neuroimaging, Radboud University,
Nijmegen, the Netherlands

Humans can recognize a scene in the blink of an eye. This gist-based visual scene perception is thought to be underpinned by specialized visual processing emphasizing the visual periphery at a cortical locus relatively low in the visual processing hierarchy. Using wide-field retinotopic mapping and population receptive field (pRF) modeling, we identified a new visual hemifield map anterior of area V2d and inferior to area V6, which we propose to call area V2A. Based on its location relative to other visual areas, V2A may correspond to area 23V described in nonhuman primates. The pRF analysis revealed unique receptive field properties for V2A: a large (FWHM $\sim 23^\circ$) and constant receptive field size across the central $\sim 70^\circ$ of the visual field. Resting-state fMRI connectivity analysis further suggests that V2A is ideally suited to quickly feed the scene-processing network with information that is not biased towards the center of the visual field. Our findings not only indicate a likely cortical locus for the initial stages of gist-based visual scene perception, but also suggest a reappraisal of the organization of human dorsomedial occipital cortex with a strip of separate hemifield

representations anterior to the early visual areas (V1, V2d, and V3d).

Introduction

Humans are remarkably apt at extracting the “gist” of a scene without analyzing its content locally (Oliva & Torralba, 2006): They can judge from flashes of only 50 ms whether the scene affords a hiding place or rather allows walking through, without awareness of its specifics like the colors or the shape of particular objects. Such gist-based visual processing is clearly at odds with the properties of conscious foveal vision that humans use to scrutinize objects. Hence, models of gist-based visual scene perception propose a type of visual processing that focuses on the visual periphery instead (Oliva & Torralba, 2006), at a cortical locus relatively low in the visual processing hierarchy. However, a visual cortical region that meets these requirements has yet to be identified.

Citation: Elshout, J. A., van den Berg, A. V., & Haak, K. V. (2018). Human V2A: A map of the peripheral visual hemifield with functional connections to scene-selective cortex. *Journal of Vision*, 18(9):22, 1–11, <https://doi.org/10.1167/18.9.22>.

<https://doi.org/10.1167/18.9.22>

Received February 28, 2018; published September 26, 2018

ISSN 1534-7362 Copyright 2018 The Authors



Previous work has thus far identified three scene-selective patches of cortex in humans: the parahippocampal place area (PPA), the transverse occipital sulcus (TOS), and retrosplenial cortex (RSC; Aguirre, Detre, Alsop, & D'Esposito, 1996; Epstein & Kanwisher, 1998; Grill-Spector, 2003). The PPA and TOS do not appear to exhibit a retinotopic emphasis toward the periphery of the visual field. The RSC is anatomically defined as Brodmann areas 29 and 30, confined between the splenium of the corpus callosum and the Parietal Occipital Sulcus (POS). The functional definition of the RSC, however, varies greatly in size across studies, with scene-selective responses labeled as RSC that often extend across the POS abutting peripheral V1 and V2d (Wolbers & Buchel, 2005; Epstein, Parker, & Feiler, 2007; Nasr et al., 2011; Huang & Sereno, 2013). As such, the term “retrosplenial complex” was introduced to distinguish it from anatomically defined RSC (Bar, 2007; Epstein, 2008). This retrosplenial complex may comprise different cortical areas, analogous to visual field maps PHC-1 and PHC-2 in functional defined PPA (Arcaro, McMains, Singer, & Kastner, 2009). For instance, Nasr et al. (2011) reported a relatively small scene-selective patch on the occipital side of the POS, abutting the peripheral representation of V1 and V2d. This particular location would not only meet the criterion of being anatomically close to the early visual areas, but also at an anatomical location that appears to exhibit representations of the visual periphery.

Previous work into a possible retinotopic organization anterior to V1 and V2d suggested the presence of an upper quadrant representation with an emphasis on the far periphery anterior to V2d (Pitzalis et al., 2006; Huang & Sereno, 2013). However, the location of this putative upper-quadrant representation differed between these studies and whether it is isolated or part of a hemifield map needs to be scrutinized. Visual field maps are typically delineated based on polar angle reversals. For instance, for the cortical representation of the central visual field, the border between V2d and V3d in the left hemisphere of the brain can be identified as those patches of cortex that represent the horizontal meridian of the visual field surrounded by two mirror-symmetric representations of the right lower quadrant of the visual field. If one would apply the same criteria to the anterior regions near the POS, however, this would lead to the conclusion that V3d and V2d are both abutted by hemifield representations. One might further expect representations of the central visual field near the parietal occipital sulcus (POS) for both hemifield representations, though in principle it would also be possible that the area does not have a focal representation of the central visual field.

Here, we used wide field retinotopic mapping (up to $\sim 45^\circ$ of eccentricity) and population receptive field

(pRF) modeling to examine the territory between areas V2d and V3d and the POS.

Methods

Subjects

Twelve healthy subjects (eight female, four male) were included in the study (ages, 21–31) following informed written consent. All subjects had normal visual acuity. The study was conducted in accordance with the Declaration of Helsinki and approved by the local ethics committee CMO Arnhem-Nijmegen.

Stimulus presentation

A custom-built visual projection system was used during retinotopic mapping to present wide-field stimuli adjusted for the 32-channel head coil and 8-channel occipital coil (field of view up to: $\sim 150^\circ \times 120^\circ$ or $\sim 90^\circ \times 90^\circ$, respectively). A detailed description can be found in the supplemental material of Arnoldussen, Goossens, and van den Berg (2011). Briefly, a projection screen was placed about 3 cm above the subject's eyes. Visual stimuli were projected onto the projection screen (32-channel: 300×150 mm or 8-channel: 143×80.5 mm) over a distance of 4.5 m by an LCD projector with custom-built optics via a mirror. Subjects wore a custom made soft convex lens with a refractive power of +30 diopters in their right eye to allow effortless sharp vision at the screen. The other eye was covered. To precisely control retinal angles, we calibrated the exact eye position relative to the presentation screen using custom methods (patent P30574US00/JKO, publication WO2013006057).

Stimulus description

Rotating wedge and an expanding ring stimuli were used for polar angle and eccentricity mapping respectively (Sereno et al., 1995). During polar angle mapping, the subject maintained fixation on a central ring while a full contrast, “wedge-shaped” checkerboard stimulus (maximum angular width of $\sim 45^\circ$) rotated counterclockwise about the center of fixation at one cycle in 64 s. For the eccentricity mapping, a radial full contrast checkerboard ring stimulus moved from the center towards the periphery of the visual field one revolution in 64 s (maximum eccentricity of $\sim 45^\circ$). No blank epochs during stimulus presentation were included. During wide field retinotopic mapping, the stimulus is often very far away from a voxel's

receptive field, and so many parts of the visual fields have mean luminance periods. For both mapping stimuli, contrast was reversed at a frequency of 2 Hz. The checks and the width of the ring-stimulus were scaled by eccentricity in accordance with the cortical magnification factor (Cowey & Rolls, 1974). Note that because of the combination of linear velocity and eccentricity scaling of the checks, receptive fields are stimulated more briefly in the foveal region compared to the periphery.

Magnetic resonance imaging

All data was collected on a 3T Siemens TRIO system at the Donders Centre for Cognitive Neuroimaging (Nijmegen, The Netherlands). A 32-channel head coil was used to obtain a high resolution full-brain anatomical scan (T1-weighted MPRAGE, 192 slices, 256×256 matrix, $1 \times 1 \times 1$ mm resolution). During the experimental scan sessions, the occipital part of the head coil with 20-channels was used to enable the wide-field screen presentation. Six subjects (6, 8–12) were scanned using an 8-channel occipital coil. High-resolution functional scans were obtained with an in-plane resolution of 2 mm iso-voxel and a slice thickness of 2 mm (T2*-weighted; multiecho echo planar imaging; 32 slices; repetition time of 2 s; echo time of 28 ms). For each subject, we collected at least two runs of each stimulus. The total duration of each run was ~ 4.5 min. Including calibration and other preparatory procedures, one scan session lasted ~ 1 hr.

Preprocessing of the imaging data

Both gray and white matter were automatically segmented using Freesurfer's recon-all pipeline (<http://freesurfer.net>). Next, the cortical surface was reconstructed at the white/gray matter border and rendered as a smoothed 3D surface (Wandell, Chial, & Backus, 2000). Motion correction between and within functional scans was applied using FSL's MCFLIRT (<http://www.fmrib.ox.ac.uk/fsl>). Next, all preprocessed data were loaded into the mrVISTA toolbox environment (<http://white.stanford.edu/software>), and the functional data were aligned with the whole-brain anatomical segmentation. Finally, the time-series data were averaged across scans, separately for each stimulus, resulting in two average-time series per subject (i.e., one for the wedge stimulus, and one for the ring stimulus), which were subsequently resampled to match the 1 mm isotropic resolution of the gray/white matter segmentation using tri-linear interpolation.

Population receptive field modeling

Population receptive field (pRF) parameters were estimated according to procedures described by Dumoulin and Wandell (2008). In brief, for each voxel, fMRI time-series predictions were generated by varying a wide range of plausible values for the parameters (x , y , and σ) of a circularly symmetric Gaussian pRF model. Optimal parameters were identified as those that minimized the residual sum of squares between the time-series data and prediction. This procedure involved a two-stage, coarse-to-fine search. First, the fMRI time-series data were smoothed along the cortical surface using a diffusion process that approximated a 5 mm FWHM Gaussian kernel, after which the pRF parameters were estimated for a subsample of the voxels and interpolated for the remaining voxels. Second, this time without smoothing, a nonlinear optimization algorithm (implemented by Matlab's "fmincon" function) was applied to every voxel whose initial parameter estimates explained more than 10% of the variance in the time-series. During both stages fMRI data were detrended using a discrete cosine transform (DCT) basis set high-pass filter (three basis functions) and converted to percent signal change by dividing by and then subtracting the mean signal amplitude over time. Finally, the best-fitting pRF model parameters were converted to polar coordinates expressed in visual angle.

Visual field map definitions

Seven visual field maps were defined in each cerebral hemisphere (for each subject separately): V1, V2v, V2d, V3v, V3d, V6, and putative area V2A. To this end, the pRF center locations were projected onto a three-dimensional rendering of each subject's brain to visualize their retinotopic maps, thresholded such that the variance explained was at least 1% (as in previous work, Pitzalis et al., 2006); this liberal threshold was used solely for the purpose of visualization/visual field map definition; in all subsequent analyses we applied the stringent inclusion criterion of at least 20% variance explained. V1, V2v, V2d, V3v, and V3d were defined according to standard procedures described elsewhere (Wandell, Dumoulin, & Brewer, 2007). The anterior border of these areas was defined as the cortical representation of the maximum stimulated eccentricity. Next, V6 and V2A were defined as hemifields directly anterior to areas V3d and V2d, respectively, using the standard criterion of polar angle reversal. Finally, the different portions of each visual area (left and right hemisphere, as well as dorsal/ventral portions for V2 and V3) were subsequently combined into a single

region-of-interest (ROI) for each area, yielding five ROIs in each subject: V1-3, V6, and V2A.

Visual field coverage maps

The visual field coverage plots of V1-3, V6, and V2A were created as follows: First, for each subject and ROI, we gathered all pRF location and width parameters for all voxels whose best-fitting pRF model explained at least 20% of the variance in the time-series. These parameters describe a two-dimensional Gaussian in the visual field. Next, we determined for each voxel, the maximum value of this Gaussian (normalized between 0 and 1) across voxels at each visual field location (pixel), thus creating a single visual field coverage image for each subject and ROI. For each ROI, these images were combined by averaging them across subjects.

Functional connectivity analysis

We conducted a functional connectivity analysis based on the resting-state data of the first 20 subjects in the publicly available WU-Minn Human Connectome Project (<http://humanconnectome.org>) Q2 dataset release (van Essen et al., 2012). We performed this analysis twice, the second time using resting-state fMRI data of the same database acquired on a different day in the same subjects. These resting-state data have been preprocessed as detailed in Smith et al. (2013), which included corrections for spatial distortions and head motion, registration to the T1w structural image, resampling to 2 mm MNI space, global intensity normalization, high-pass filtering with a cut-off at 2000 s, and the FIX artifact removal procedure (Griffanti et al., 2014; Salimi-Khorshidi et al., 2014). For this work, we additionally smoothed the images using a 6 mm FWHM Gaussian kernel, applied a 100 s cut-off high-pass filter, and also removed the mean ventricular and white-matter signal from the time-series data. After normalizing the time-series of each voxel to zero mean and unit variance, the data were concatenated, resulting in two 30-min functional scans per subject. Next, we defined three spherical seed regions of 10 mm diameter. The first seed was centered at MNI coordinates ($x = 8/-8$, $y = -96$, $z = 14$) corresponding to visual area V2d. The second seed was centered at MNI coordinates ($x = 8/-8$, $y = -76$, $z = 24$) abutting the parietal occipital sulcus (POS), corresponding to visual area V2A. The third seed was centered at MNI coordinates ($x = 10/-8$, $y = -82$, $z = 36$) abutting the POS, corresponding to visual area V6. For each session separately, we then calculated the unique functional connectivity of each seed region using the FSL's sbca tool (O'Reilly,

Beckmann, Tomassini, Ramnani, & Johansen-Berg, 2010). As such, the first eigenvariate of the time-series in each seed region was correlated with the voxel-wise time-series in the rest of the brain, controlled for the eigenvariate of the time-series in the other seeds (i.e., by regressing out the eigenvariate time-series of the remaining two seed regions from the first and the rest of cortex). The ensuing subject-level partial correlation maps were subsequently Fisher z -transformed and subjected to a one-sample permutation t test with threshold-free cluster enhancement (TFCE; Smith & Nichols, 2009) using FSL's randomize tool (5000 permutations) to characterize the connectivity maps of each seed region in terms of maps of the ensuing voxel-wise t statistics. These maps were subsequently thresholded at a significance level of $p < 0.05$ (FWE corrected).

Results

We recorded fMRI data of twelve healthy participants during a wide-field retinotopic mapping session and fitted a circular symmetric Gaussian pRF model to the ensuing voxel-wise time-series data. The pRF estimates, explaining on average 45% of time-series variance, provided converging evidence of two abutting hemifield representations at the anterior end of areas V2d and V3d (Figures 1 and 2). Though there is variability across subjects due to methodological challenges associated with wide field retinotopic mapping of an area deep inside the POS, careful inspection of each individual hemisphere shows that the border between these hemifields was formed by a polar-angle reversal at the representation of the upper vertical meridian, just as for instance the border between V1 and V2.

A reversal in the eccentricity map further appeared to distinguish the hemifield maps from its bordering lower tier region V2d or V3d (see Figure 3, which summarizes the relationship between eccentricity and cortical distance through V2d and V2A from the occipital pole to the posterior occipital sulcus based on voxels, whose best fitting pRF model exceeded 20% variance explained). Notably, the anterior border of V2d and V3d coincided with the appearance of an upper visual field representation anterior to V2d and V3d. On both sides of the borders of V2d and V3d, eccentricity rapidly decreased away from these borders, with a much slower decrease posteriorly closer to the fovea (due to the cortical magnification factor in areas V2d and V3d). The hemifield anterior of V3d corresponds to putative human area V6 as described previously (Pitzalis et al., 2006). The hemifield representation anterior to V2d seems to overlap with

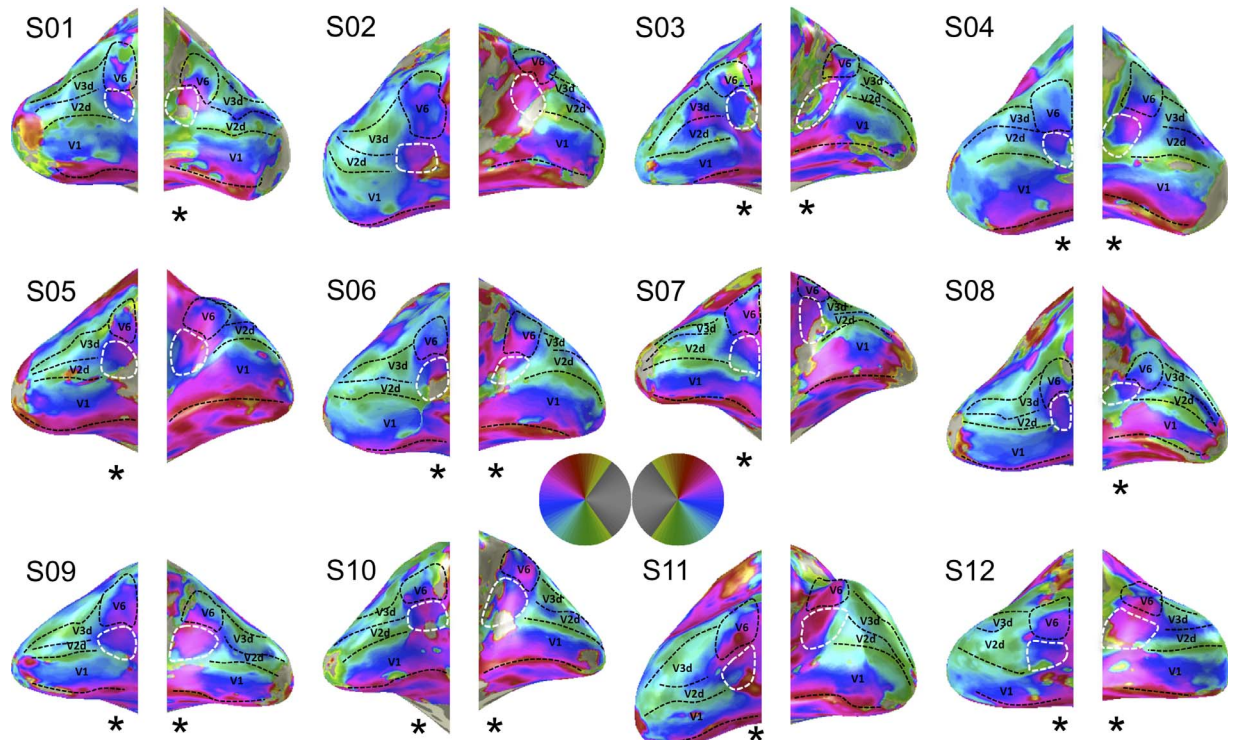


Figure 1. Wide-field retinotopic mapping results for all twelve subjects. Shown are polar angle maps. The borders between V1, V2, and V3 are indicated by the dashed black lines. V2A is enclosed by a dashed white line and can be found inferior to area V6 at the anterior end of V2d. V6 is enclosed by the dashed black line. The asterisks beneath the hemispheres indicate if we can identify the hemifield representation after careful inspection of the figure (17 of the 24 hemispheres in 11 of the 12 participants). Note in four of the other seven hemispheres we can identify an upper field representation only (S2 left hemisphere, S5 right hemisphere, S8 left hemisphere, and S11 right hemisphere).

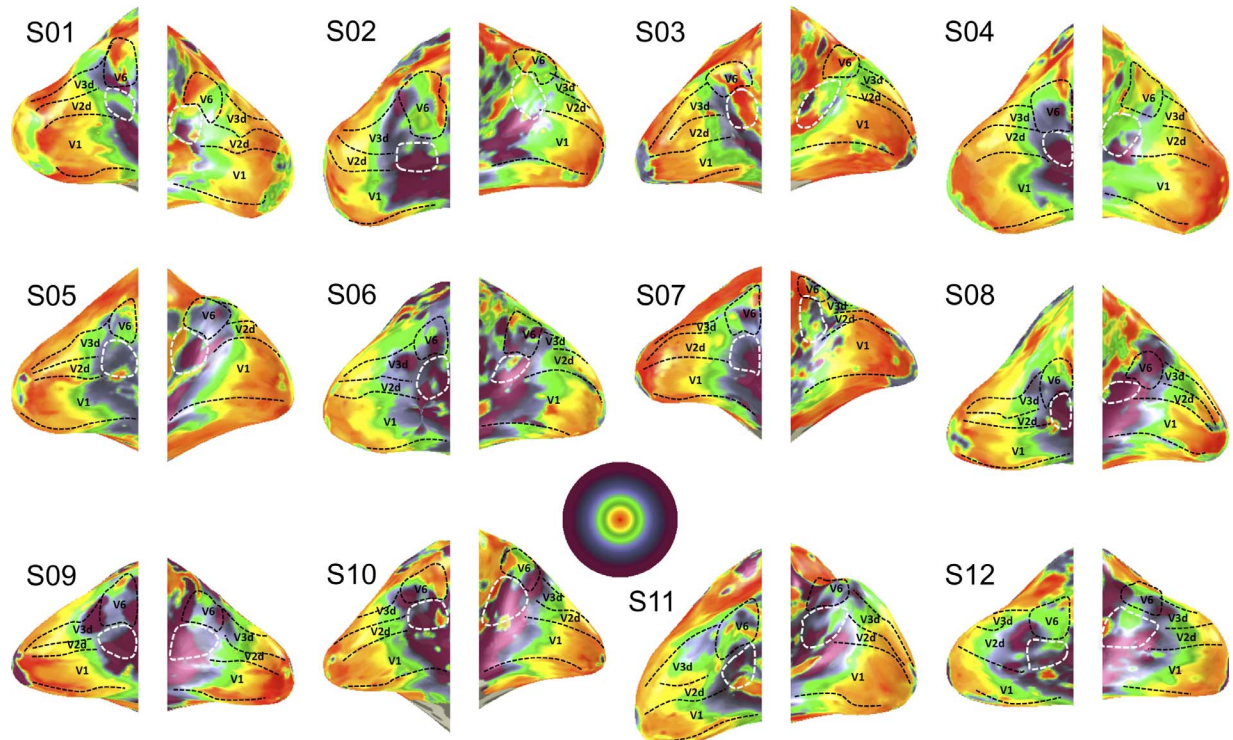


Figure 2. Eccentricity maps shown for all twelve subjects. Maximum stimulus coverage is $\sim 45^\circ$.

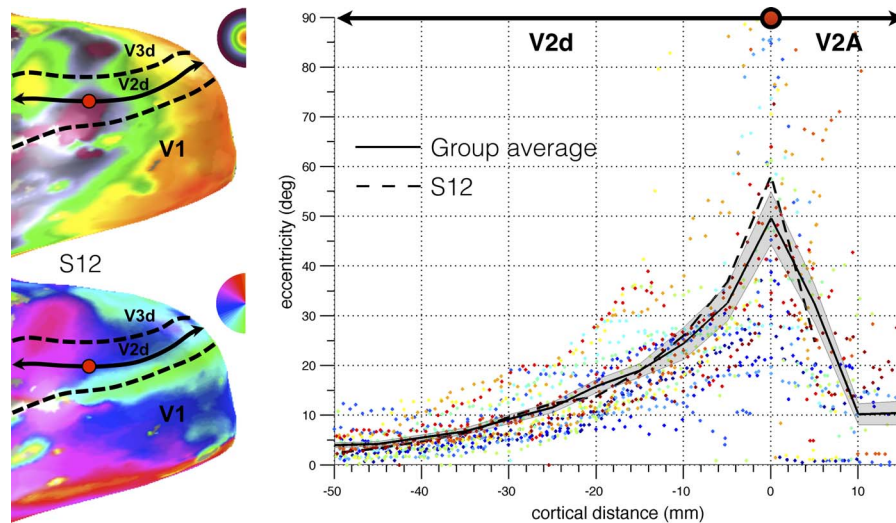


Figure 3. Reversal in eccentricity as a function of the cortical distance along a line (illustrated for S12 in the left panel) that followed the cortical surface from the foveal representation of V2d all the way to the POS (bins of 5 mm). For each subject (plotted in different colors), cortical distance was calculated with respect to the point of maximum eccentricity such that distances in the posterior direction were negative and distances in the anterior direction were positive. The solid black line represents the data of the group average. The shaded area represents the standard error of the mean. Note that the eccentricity color map is linearly scaled in contrast to Figure 2, which has logarithmic scaling.

the upper field quadrant reported by Pitzalis et al (2006), and part of the retrosplenial complex (Nasr et al., 2011; Huang & Sereno, 2013). We propose to call this hemifield representation anterior to V2d and inferior to V6, area V2A.

To examine V2A's representation of the visual field in more detail, coverage plots were created based on the most reliable pRF parameter estimates (i.e., pRF models whose explained variance exceeded 20%) for all defined visual field maps (V1, V2, V3, V6, V2A). This method allows for a quantitative inspection of the visual field maps illustrated in figures 1 and 2. The coverage plots (Figure 4) show clear evidence that area

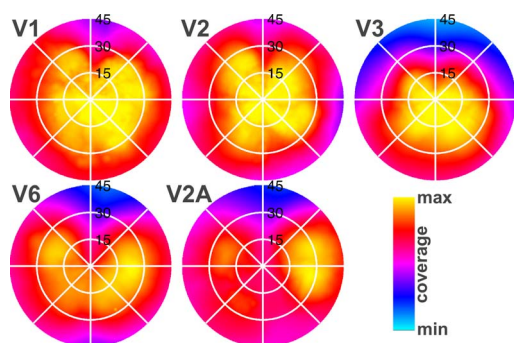


Figure 4. Average visual field coverage maps for receptive fields of paired ROIs (ventral and dorsal quadrants combined for V1–V3) from the two hemispheres represent the entire visual field (0° – 45°), indicating that V2A also represents a hemifield emphasizing the visual periphery, like V6. Yellow indicates that field coverage for these areas is found in all subjects (100%).

V2A has a complete hemifield representation. The red color in Figure 4 indicates that there's >80% field coverage found across subjects. This is in line with the polar angle maps illustrated in Figure 1. In contrast to V1–V3 whose visual field coverage is biased towards the center of the visual field, both V6 and V2A exhibited coverage of a complete hemifield with an emphasis on the periphery of the visual field (Figure 4).

Our approach of combining wide field visual stimulation and pRF analysis further allowed us to study for the first time the eccentricity dependency of pRF size estimates at high eccentricities in human subjects. We determined the relationship between the pRF size estimates and eccentricity by gathering for each visual field map all voxels across all subjects whose pRF predicted more than 20% of the variance and then binning these into segments of 5° eccentricity (Figure 5a and b). In line with previous work that mapped the central $\sim 15^{\circ}$ of the visual field, pRF size estimates in V1–V3 and V6 increase linearly with eccentricity when measuring up to 45° of eccentricity. Interestingly, however, the expected linear increase in pRF size with eccentricity could not be observed for V2A, as V2A's pRF size was very large even at very small eccentricities (FWHM $\sim 23^{\circ}$) and did not change systematically across the central $\sim 70^{\circ}$ of the visual field ($t_{11} = -0.56$, $p = 0.59$; one-sample t test for a nonzero slope of the regression line). Of note is also that the pRF centers in V2A extend all the way down to at least 2.5° eccentricity even though V2A abuts the peripheral representations of anterior V2d, which indicates that V2A has its own representation of the central visual field.

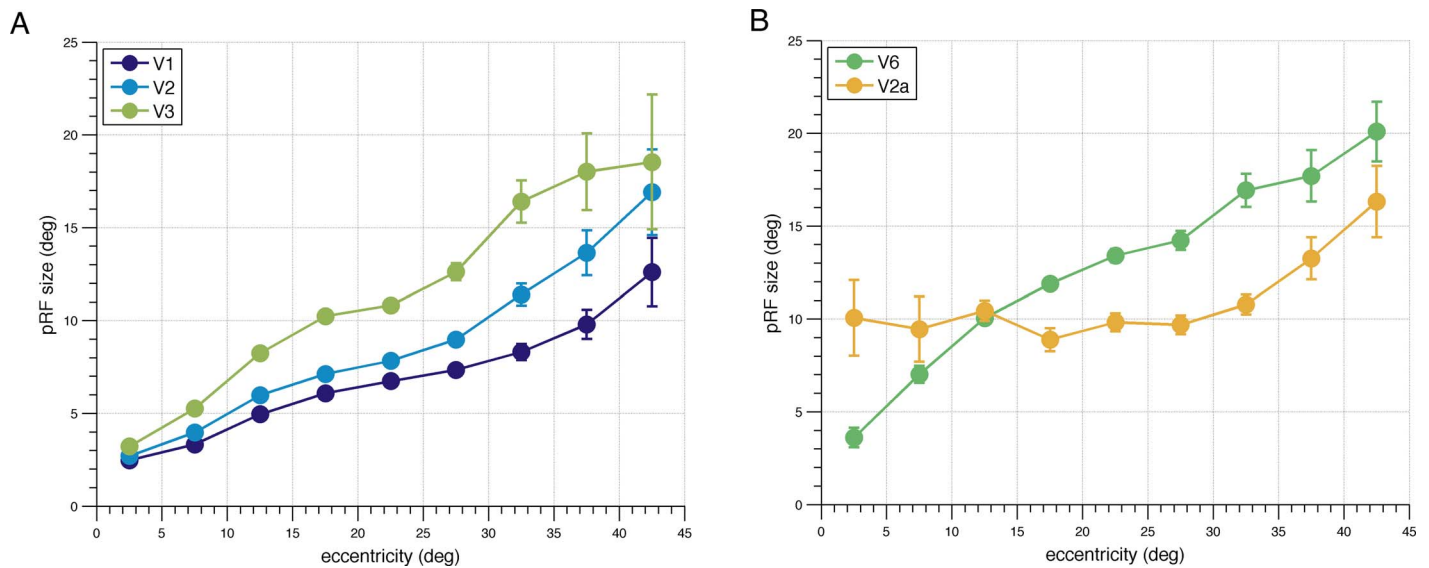


Figure 5. pRF size versus eccentricity function (5° bins). (A) Data averaged across all participants for V1, V2, and V3 and (B) V2A and V6. Error bars represent standard errors.

To determine the functional relevance of the new visual area V2A, we performed a seed-based functional connectivity analysis on the resting-state data of the first 20 subjects in the publicly available WU-Minn Human Connectome Project (<http://humanconnectome.org>) Q2 dataset release (van Essen et al., 2012). As a measure of functional connectivity, we used the correlation between the resting-state fMRI time-series of one region (V2A, V6, or V2d) and the rest of the brain, while controlling

for the fMRI activity in the remaining two regions. In line with anatomical tract tracer injections in experimental animals, this revealed that area V6 is part of a lateral occipital, parietal, and premotor network (Galletti et al., 2001), and that V2d is functionally connected with visual cortex exclusively (Figure 6). By contrast, area V2A appeared to be part of a network including the parahippocampus, transverse occipital sulcus (TOS), and retrosplenial cortex (RSC), which has previously

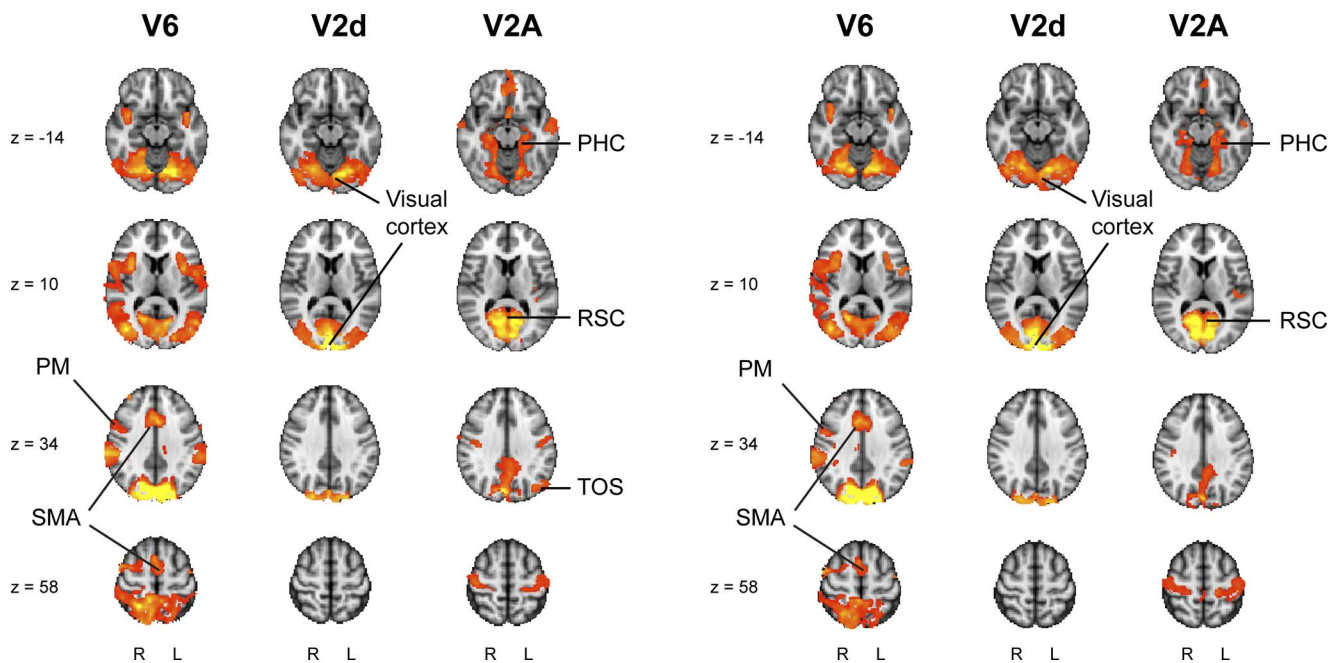


Figure 6. Seed-based partial correlation analysis results for V6, V2d, and V2A (left panel). Maps of the t statistic are thresholded at $p < 0.05$ (FWE corrected). These results were replicated using resting-state fMRI data acquired on a different day in the same subjects (right panel). PM = Pre Motor area; SMA = Supplementary Motor Area; PHC = Parahippocampal Cortex; RSC = Retrosplenial Cortex; TOS = Transverse Occipital Sulcus.

been shown to be involved in scene perception (Epstein et al., 2007; Figure 6).

Discussion

By combining wide field retinotopic mapping and pRF modeling, we found a new visual hemifield representation, which we propose to call area V2A. V2A emphasizes the visual periphery, is located anterior to V2d and inferior to V6, and exhibits large, constant sized receptive fields across all eccentricities tested. In addition, we presented evidence to suggest that V2A plays a crucial role in visual scene perception based on its functional connectivity patterns with scene-selective cortex. V2A's role in visual scene perception may also be gleaned from its proximity to (and perhaps overlap with) the occipital parts of the retrosplenial complex (RSC) reported in earlier work (Nasr et al., 2011; Huang & Sereno, 2013). Indeed, it is possible that V2A is one of several different functional areas within the RSC (Bar, 2007; Epstein, 2008; Solomon & Rosa, 2014). In nonhuman primates like the Marmoset, several hemifield areas border the anterior region of dorsal V1 and V2 (Rockland, 2012; Yu, Chaplin, Davies, Verma, & Rosa, 2012; Solomon & Rosa, 2014; Yu, Chaplin, & Rosa, 2015). Of these areas, prostriata and area 23V are considered part of the RSC-complex and have been associated with peripheral scene monitoring. Mikellidou et al. (2017) recently mapped the human prostriata anterior to V1. Based on its position relative to the other visual areas (anterior to V2d, inferior to V6, and superior to human prostriata), it appears likely that V2A corresponds to area 23V. Indeed, according to Solomon and Rosa (2014, page 11), "Based on its location relative to V2, area 23V seems to correspond to the scene-selective area of the retrosplenial cortex described by Nasr et al. (2011) in other species."

Area V2A also appears to overlap partly with area DVT defined in a recent multimodal parcellation of human cortex (Glasser et al., 2016). Area DVT, however, is more elongated than V2A, extending from Prostriata all the way anterior to V6. We are reluctant to interpret this discrepancy because the multimodal parcellation did not incorporate retinotopic mapping data and because the multimodal parcellation beyond early visual cortex does not adhere very well to well-established retinotopic mapping results. For instance, while early visual areas V1–3 are correctly delineated, visual areas such as hV4 and LO are rather poorly delineated by the multimodal parcellation (see e.g., supplement s3, figure 3 of Glasser et al., 2016).

Our seed-based functional connectivity analysis indicates that area V2A is part of a scene selection network including PPA, TOS, and RSC, while area V6

is part of a lateral occipital, parietal, and premotor network. While the latter is in line with anatomical tract tracer injections in the macaque (Galletti et al., 2001), it may appear inconsistent with recent results of Tosoni et al. (2015), who observed functional connections between V6 and PPA. It is of note, however, that Tosoni et al. (2015) based their functional connectivity characterizations on full correlations, while ours was based on partial correlations (controlling for the activity of neighboring regions). It is likely, therefore, that the functional connectivity between V6 and PPA observed by Tosoni et al. (2015) reflects indirect connectivity via V2A (since in the present work, V2A exhibited significant partial correlation with PPA after regressing out the activity in V6).

Mikellidou et al. (2017), who recently reported on human prostriata, did not examine this area's receptive field size. A general feature of receptive field organization that can be observed across many visual areas and species is that the receptive field size increases with eccentricity. By contrast, V2A's receptive field size appears to be constant up to about 35° eccentricity. A similar feature has also been observed in Marmoset prostriata (Yu et al., 2012) and may facilitate extracting the statistical structure of a scene because it allows for sampling the retinal image with equal resolution across the visual field. A constant receptive field size may further be useful for accounting for gaze movements. If V2A's purpose is to rapidly extract the gist of a scene to provide a context for further image processing, it could be beneficial to additionally keep track of the displacement of subsequent snapshots as we move our eyes and head. In this way, it would be possible to place the individual snapshots in the larger context of our surrounding environment (Robertson, Hermann, Myrick, Kravitz, & Kanwisher, 2016). Previous work has shown that sampling the retinal image with relatively large receptive fields (blur) allows for a straightforward computation of its partial spatial derivatives of any order (Koenderink & Van Doorn, 1987). As such, gaze shifts can be estimated by local "shifter" circuits (Olshausen, Anderson, & Van Essen, 1993) directly from the visual input up to a saccade size that is determined by the receptive field (or blur) size and the order of differentiation (Beintema & Van den Berg, 1998). In principle, these shifter circuits can be implemented in any visual area with nonzero receptive field sizes, but if the receptive field size increases with eccentricity, this would put a limit to the size of the gaze-displacements that can be estimated based on information from the center of the visual field, leading to different displacement estimates across the visual field. By virtue of its constant receptive field sizes, therefore, V2A may be ideally suited to rapidly extract the global displacement of the image when we move our heads and eyes. If so, we estimate that V2A can keep track of gaze movements of

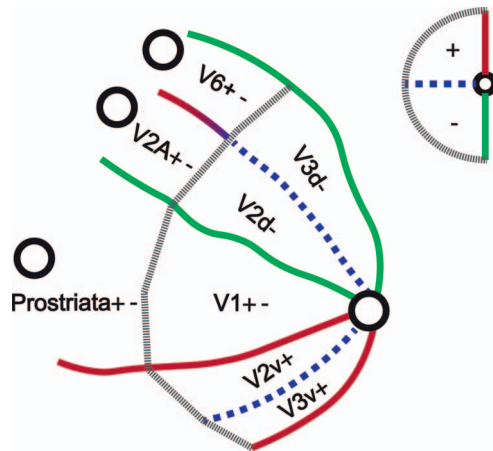


Figure 7. Model of the human dorsal visual cortex. The primary visual areas are abutted by hemifield representations which emphasize the visual periphery. Pitzalis et al (2006) discovered V6 anterior to V3d. Recently Mikellidou et al. (2017) mapped prostriata anterior to V1. In this paper we revealed area V2A anterior to V2d for the first time.

up to at least about half the receptive field diameter (i.e., $\sim 15^\circ$; Beintema & Van den Berg, 1998). This extent covers the majority of the prior probability distribution of saccades in retinocentric space (Tatler & Vincent, 2009), suggesting that V2A can account for the most frequent types of gaze-shifts.

Together with the recent discovery of human prostriata, the present findings suggest a reappraisal of the organization of human dorsomedial occipital cortex with a strip of separate hemifield representations anterior to the early visual areas (Figure 7). The strip of contralateral hemifield representations consists of areas V6 (as described by, for example, Pitzalis et al., 2006) at the anterior end of area V3d, Prostriata as described by Mikellidou et al. (2017) at the anterior end of V1 and area V2A at the anterior end of V2d. The strip of hemifield representations anterior to dorsal V1–V3 reveals an interesting alignment between the human and the Marmoset literature.

It is challenging to map visual areas in this region of the cortex deep inside the POS. Whereas the summary plots show convincing evidence of V2A, the individual data show substantial variability. Inconsistencies in the polar angle and eccentricity maps are likely due to the challenges associated with mapping a visual area with predominantly far peripheral responses, leading to a poorer characterisation of different portions of the maps in some subjects. Furthermore, our wide-field retinotopic mapping paradigm comes at the expense of accurately mapping the central $\sim 5^\circ$ of the visual field, which explains the inconsistencies regarding the central visual field representation. Finally, the maps presented in Figures 1 and 2 only show the pRF centre positions, but a voxel's response depends on a larger area because

the pRF is not a point but a circular region with a size. Looking at figure 5, we can see that V2A voxels have very large pRFs, so for a voxel to respond to the centre of the visual field, it does not need a pRF that is positioned at the very centre of the visual field.

In conclusion, our data provide converging evidence of a distinct hemifield representation at the anterior end of V2d, which we propose to call area V2A. Area V2A is characterized by unique receptive field properties such as a constant receptive field size across the central $\sim 70^\circ$ of the visual field and exhibits unique functional connectivity patterns with a network of regions that have previously been related to scene processing. V2A may correspond to marmoset area 23V, which also lies anterior to V2d near the parietal occipital sulcus, features large receptive fields, and has been associated with visual scene processing. Together, these features suggest that V2A supports the initial, gist-based stages to visual scene perception in humans.

Keywords: fMRI, retinotopic mapping, pRF modeling, scene perception, gist

Acknowledgments

We thank D. Bergsma, S. Vinks, and D. Arnoldussen for help with data collection. This work was supported by Netherlands Organization for Scientific Research (NWO ZonMW-InZicht grant 94309003 to A.V.v.d.B.). K.V.H. is supported by the Netherlands Organisation for Scientific Research (NWO 016.Veni.171.068). The resting-state fMRI data were provided by the Human Connectome Project, WU-Minn Consortium (Principal Investigators D.C. Van Essen and K. Ugurbil; 1U54MH091657) funded by the 16 NIH institutes and Centers that support the NIH Blueprint for Neuroscience Research, and by the McDonnell Center for Systems Neuroscience at Washington University.

Commercial relationships: none.

Corresponding author: Joris A. Elshout.

Email: j.elshout@donders.ru.nl.

Address: Department of Cognitive Neuroscience, Radboud University Medical Centre, and Donders Institute for Brain, Cognition and Behaviour, Centre for Cognitive Neuroimaging, Radboud University, Nijmegen, the Netherlands.

References

Aguirre, G. K., Detre, J. A., Alsop, D. C., & D'Esposito, M. (1996). The parahippocampus

- suberves topographical learning in man. *Cerebral Cortex*, 6, 823–829.
- Arcaro, M. J., McMains, S. A., Singer, B. D., & Kastner, S. (2009). Retinotopic organization of human ventral visual cortex. *The Journal of Neuroscience: The Official Journal of the Society for Neuroscience*, 29, 10638–10652.
- Arnoldussen, D. M., Goossens, J., & van den Berg, A. V. (2011). Adjacent visual representations of self-motion in different reference frames. *Proceedings of the National Academy of Sciences, USA*, 108, 11668–11673.
- Bar, M. (2007). The proactive brain: Using analogies and associations to generate predictions. *Trends in Cognitive Sciences*, 11, 280–289.
- Beintema J. A., & Van den Berg A. V. (1998). Heading detection using motion templates and eye velocity gain fields. *Vision Research*, 38, 155–179.
- Cowey, A., & Rolls, E. T. (1974). Human cortical magnification factor and its relation to visual acuity. *Experimental Brain Research*, 21, 447–454.
- Dumoulin, S. O., & Wandell, B. A. (2008). Population receptive field estimates in human visual cortex. *Neuroimage*, 39, 647–660.
- Epstein, R. A. (2008). Parahippocampal and retrosplenial contributions to human spatial navigation. *Trends in Cognitive Sciences*, 12, 388–396.
- Epstein, R. A., Higgins, J. S., Jablonski, K., & Feiler, A. M. (2007). Visual scene processing in familiar and unfamiliar environments. *Journal of Neurophysiology*, 97, 3670–3683.
- Epstein, R. A., & Kanwisher, N. (1998, April 9). A cortical representation of the local visual environment. *Nature*, 392, 598–601.
- Epstein, R. A., Parker, W. E., & Feiler, A. M. (2007). Where am I now? Distinct roles for parahippocampal and retrosplenial cortices in place recognition. *The Journal of Neuroscience*, 27, 6141–6149.
- Galletti, C., Gamberini, M., Kutz, D.F., Fattori, P., Luppino, G., Matelli, M. (2001). The cortical connections of area V6: An occipito-parietal network processing visual information. *The European Journal of Neuroscience*, 13, 1572–1588.
- Glasser, M. F., Coalson, T. S., Robinson, E. C., Hacker, C. D., Harwell, J., Yacoub, E., ... van Essen, D. C. (2016, August 11). A multi-modal parcellation of human cerebral cortex. *Nature*, 536, 171–178.
- Griffanti L., Salimi-Khorshidi, G., Beckmann, C. F., Auerbach, E. J., Douaud, G., Sexton, G. E., ... Smith, S. M. (2014). ICA-based artefact removal and accelerated fMRI acquisition for improved resting state network imaging. *Neuroimage*, 95, 232–247.
- Grill-Spector, K. (2003). The neural basis of object perception. *Current Opinion in Neurobiology*, 13(2), 159–166.
- Huang, R. S., & Sereno, M. I. (2013). Bottom-up retinotopic organization supports top-down mental imagery. *The Open Neuroimaging Journal*, 7, 58–67.
- Koenderink J. J., & Van Doorn A. J. (1987). Representation of local geometry in the visual field. *Biological Cybernetics*, 55, 367–375.
- Mikellidou, K., Kurzawski, J. W., Frijia, F., Montanaro, D., Greco, V., Burr, D. C., & Morrone, M. C. (2017). Area prostriata in the human brain. *Current Biology*, 27, 1–5.
- Nasr, S., Liu, N., Devaney, K. J., Yue, X., Rajimehr, R., Ungerleider, L. G., & Tootell, R. B. H. (2011). Scene-selective cortical regions in human and non-human primates. *The Journal of Neuroscience*, 31, 13771–13785.
- Oliva, A., & Torralba, A. (2006). Building the gist of a scene: The role of global image features in recognition. *Progress in Brain Research*, 155, 23–36.
- Olshausen B. A., Anderson C. H., & Van Essen, D. C. (1993). A neurobiological model of visual attention and invariant pattern recognition based on dynamic routing of information. *The Journal of Neuroscience*, 13, 4700–4719.
- O'Reilly, J. X., Beckmann, C. F., Tomassini, V., Ramnani, N., & Johansen-Berg, H. (2010). Distinct and overlapping functional zones in the cerebellum defined by resting state functional connectivity. *Cerebral Cortex*, 20, 953–965.
- Pitzalis, S., Galletti, C., Huang, R-S., Patria, F., Committeri, G., Galati, G., ... Sereno, M. I. (2006). Wide-field retinotopy defines human cortical visual area V6. *The Journal of Neuroscience*, 26, 7962–7973.
- Robertson, C. E., Hermann, K. L., Mynick, A., Kravitz, D. J., & Kanwisher, N. (2016). Neural representations integrate the current field of view with the remembered 360° panorama in scene-selective cortex. *Current Biology*, 26, 2463–2468.
- Rockland, K. S. (2012). Visual system: Prostriata—a visual area off the beaten path. *Current Biology*, 22, 571–573.
- Salimi-Khorshidi G., Douaud, G., Beckmann, C. F., Glasser, M. F., Griffanti, L., & Smith, S. M. (2014). Automatic denoising of functional MRI data: Combining independent component analysis and hierarchical fusion of classifiers. *Neuroimage*, 90, 449–468.

- Sereno, M. I., Dale, A. M., Reppas, J. B., Kwong, K. K., Belliveau, J. W., Brady, T. J., Rosen, B. R., & Tootell, R. B. H. (1995, May 12). Borders of multiple visual areas in humans revealed by functional magnetic resonance imaging. *Science*, *12*, 889–893.
- Smith, S. M., Beckmann, C. F., Andersson, J., Auerbach, E. J., Bijsterbosch, J., Douaud, G., . . . Glasser, M. F. (2013). Resting-state fMRI in the human connectome project. *Neuroimage*, *80*, 144–168.
- Smith, S. M., & Nichols, T. E. (2009). Threshold-free cluster enhancement: Addressing problems of smoothing, threshold dependence and localisation in cluster inference. *Neuroimage*, *44*, 83–98.
- Solomon, S. G., & Rosa, M. G. P. (2014). A simpler primate brain: The visual system of the Marmoset monkey. *Frontiers in Neural Circuits*, *8*:e96.
- Tatler, B. W., & Vincent, B. T. (2009). The prominence of behavioural biases in eye guidance. *Visual Cognition*, *17*, 1029–1054.
- Tosoni, A., Pitzalis, S., Committeri, G., Fattori, P., Galletti, C., & Galati, G. (2015). Resting-state connectivity and functional specialization in human medial parieto-occipital cortex. *Brain Structure and Function*, *220*, 3307–3321.
- van Essen, D. C., Ugurbil, K., Auerbach, E., Barch, D., Behrens, T. E. J., Bucholz, R., . . . Yacoub, E. (2012). The human connectome project: A data acquisition perspective. *Neuroimage*, *62*, 2222–2231.
- Wandell, B. A., Chial, S., & Backus, B. T. (2000). Visualization and measurement of the cortical surface. *Journal of Cognitive Neuroscience*, *12*, 739–752.
- Wandell, B. A., Dumoulin, S. O., & Brewer, A. A. (2007). Visual field maps in human cortex. *Neuron*, *56*, 366–383.
- Wolbers, T., & Buchel, C. (2005). Dissociable retrosplenial and hippocampal contributions to successful formation of survey representations. *The Journal of Neuroscience*, *25*, 3333–3340.
- Yu, H.-H., Chaplin, T. A., Davies, A. J., Verma, R., & Rosa, M. G. P. (2012). A specialized area in limbic cortex for fast analysis of peripheral vision. *Current Biology*, *22*, 1351–1357.
- Yu, H.-H., Chaplin, T. A., & Rosa, M. G. P. (2015). Representation of central and peripheral vision in the primate cerebral cortex: Insights from studies of the Marmoset brain. *Neuroscience Research*, *93*, 47–61.